ELSEVIER

Applied Mathematical Modelling 22 (1998) 601–627

APPLIED MATHEMATICAL MODELLING

Mechanics of Pb40/Sn60 near-eutectic solder alloys subjected to vibrations

Cemal Basaran *, Rumpa Chandaroy

Department of Civil Engineering, Electronic Packaging Laboratory, State University of New York at Buffalo, 212 Ketter Hall, Buffalo, NY 14260-4300, USA

Received 20 January 1997; received in revised form 19 May 1998; accepted 2 June 1998

Abstract

Pb40/Sn60 is the most commonly used solder alloy for microelectronics packaging. It is well understood that, heat generated by the circuits when a semiconductor device is on and the coefficient of thermal expansion mismatch between the soldered layers lead to the thermal fatigue of the solder joints. On the other hand, there is very little research done to understand failure mechanics of solder joints when microelectronics devices are subjected to vibrations. In this study, it is shown that dynamic stresses contribute to the failure mechanism and in certain circumstances they can become the dominant failure cause when semiconductor devices are used in a vibrating environment. The purpose of this study is to understand the mechanics of the vibration induced damage in solder interconnects. A material nonlinear time domain dynamic analysis of a solder joint was performed using a damage mechanics based constitutive model. The analysis was done for isothermal condition and no thermal loads were considered. The study included a wide range of frequency and acceleration combinations.

Keywords: Electronic packing; Solder joint; Vibration

1. Introduction

Due to shrinking device size and increasing number of VLSI circuits in a chip, Surface Mount Technology (SMT) has become the most popular packaging in the microelectronics industry. By using the entire area under the semiconductor device, the SMT provides more space for I/O interconnections, thereby increasing the interconnection density per unit area of the package. As a result, the use of surface mounting components with solder joints is steadily increasing. Pb40/Sn60 near eutectic solder alloy is the most commonly used solder joint bonding material due to its low melting point (183°C), ease of manufacturing, good bonding strength and low cost. Steinberg (1988) reports that "solder is so important in this [microelectronic packaging] process that many people in the industry claim that the reliability of the electronic equipment amounts to the reliability of the solder joints".

In a microelectronics device the solder joint provides electrical and thermal continuity as well as structural integrity. It is well known that the dominant failure mode for solder joints is low

* Corresponding author. Tel.: +1 716 645 2114/2429; fax: +1 716 645 3733; e-mail: cjb@ eng.buffalo.edu.

ISSN/98/$ – see front matter
PII: S0307-904X(98)10059-8

cycle thermal fatigue and this subject has been studied extensively. On the other hand, the literature is scarce regarding how vibrations affect fatigue life of solder joints. This is probably due to the fact that, according to the popular opinion, dynamic loading is believed to cause elastic strains only and makes a secondary contribution to the fatigue damage (Blanks, 1976; Markstein, 1987; Steinberg, 1988; Suhir and Lee, 1988; Barker et al., 1990; Pitarresi and Akanda, 1993; Lau et al., 1995; Barker and Sidharth, 1995; Darbha et al., 1996).

The only paper in the literature that discusses solder joint mechanics under vibrations considering solder material nonlinearity was published by Barker et al. (1990). The authors presented a generalized strain versus life approach model for combined vibrational and thermal fatigue of solder joints in which their results strongly suggest that strains caused by vibrations must be included in any reliability prediction model developed for solder joint reliability.

In this study in order to study the dynamic behavior of solder joints, a damage mechanics based constitutive model is developed and implemented in a finite element procedure. The proposed model takes into account, time dependent creep-damage, grain size, microstructure and temperature dependence.

In many applications microelectronic devices are used in environments where they are subject to vibrations, such as in military or automotive applications. An examination of the documentation available from some component manufacturers and from publications such as MIL-STD-883 (MIL-HDBK, 1964) show that components are typically rated for 20-g peak sinusoidal vibrations, 1500 g of shock using a 0.005 s (200 Hz) half-sine shock pulse, and 30,000 g of acceleration for small semiconductor devices. Acceleration levels of 100 g or more are quite common in military electronic systems (Steinberg, 1988).

The frequency of the thermal cycles for semiconductor devices ranges from five cycles per minute in telecommunications equipment to one cycle per day in personal computer processors (Barker et al., 1990). The frequency range for harmonic vibrations for most vehicle and equipment is 1–5000 Hz (Suhir and Lee, 1988).

The standard practice in the electronics industry today is to use common electronic components in severe vibration and shock environments that often far exceed the ratings of these components (Steinberg, 1988). This is done because it is too expensive to run high-acceleration level tests on so many different components (Steinberg, 1988). Performing computer simulations instead of laboratory tests to predict reliability of these components would be very beneficial to the microelectronics industry. Commercially available general purpose finite element programs such as ANSYS, ABAQUS, ADINA (ANSYS, 1992; ABAQUS, 1996; ADINA, 1996), cannot perform damage mechanics analysis under any load conditions. Therefore, there is a need for damage mechanics based constitutive models and finite element procedures that can simulate behavior of solder alloys under variable load conditions.

The constitutive model and the finite element procedure proposed in this paper can be used to mitigate the need to run these expensive high-acceleration tests. Computer simulation of the dynamic behavior of the solder joints in surface mount packaging could be used to understand the behavior at acceleration levels that are too difficult or too expensive to obtain in the laboratory. A numerical analysis procedure can also be used to perform a parametric study on a new package interconnect without having to build a prototype for every possible configuration.

2. Constitutive modelling

It is well known that near eutectic Pb/Sn solder alloy is a very complex material (Frear et al., 1994; Morris and Reynolds, 1992). The thermo-mechanical properties and behavior of a

particular solder joint depend on its microstructure. Microstructure depends on the cooling rate, age, temperature, initial deformations due to manufacturing and the deformation history. For example, for Pb40/Sn60 Young's modulus values of 9–48 GPa have been reported in the literature (Knecht and Fox, 1990; Basaran et al., 1998a, b). One of the reasons for this discrepancy is that near eutectic solder alloy changes it mechanical behavior as it undergoes deformations or temperature changes (Stone and Rashid, 1994). The variation in the mechanical behavior is also due to the fact that near eutectic Pb/Sn solder alloys are thermodynamically unstable materials. This is best described by Morris et al. (1994), "Good solders are low-melting [point] alloys and hence, are ordinarily eutectics or other two-phase mixtures. They bond to substrate by reacting chemically to form intermetallic compounds. They are ordinarily used in the as-solidified or slightly aged condition. These factors ordinarily lead to a microstructure that is thermodynamically unstable. As the joint is aged, thermally cycled or deformed, its microstructure evolves [coarsens to increase its grain size] so that its mechanical behavior changes with time." Formulating this coarsening is very complex and needs further extensive studies. Morris et al. (1994) conclude that, "At the present state of knowledge, it is not possible to represent these [microstructural evolution] in an accurate analytical model." The constitutive model proposed in this paper can predict the macroscopic global behavior of a solder joint but not its microstructural evolution.

Therefore, using Pb/Sn solder alloy mechanical properties from the literature to design a microelectronics package solder joint is not recommended. The mechanical properties of the solder joint used in the design must be identical to those of the manufactured joints. Otherwise analysis results may be misleading. Hence, it is recommended that thermomechanical material properties are obtained from a solder joint in a manufactured microelectronics package (Morris and Reynolds, 1992).

In addition, Bonda and Noyan (1996) have shown that mechanical properties are dependent on the size of the specimen. Therefore, it is imperative that samples tested are the same size as the solder joints in the microelectronics device that is being designed. Unfortunately, due to difficulties measuring strain on micron scale specimens, presently only bulk solder properties are used to design solder joints.

Pb40/Sn60 is a two phase alloy, it has been shown that tin and lead phases have different responses. Bonda and Noyan (1996) and Frear et al. (1995) report that, at the beginning tin phase dominates the mechanical behavior and lead phase dominates the behavior when the solder joint is near failure. It is well known that characteristic size of the lead rich phase regions correlate with strain localization and subsequent failure. The constitutive model proposed in this paper can characterize this two phase behavior, accurately.

The Disturbed State Concept (DSC) is used to develop the constitutive model used in this study. The DSC is a material (and interface) modeling approach which assumes that the material is inhomogeneous and it is a two phase mixture, intact and damaged.

Solder alloys are usually heterogeneous, and often have flaws/discontinuities that form during the reflow process. The solder material cannot therefore be treated as a continuum. Hence, it is necessary to introduce the discontinuous nature of the material into the constitutive model. When the solder joint is subjected to cycling shear strain due to thermal effects and/or vibrations, microstructural changes [dislocations] take place in the solder. Initially, the material response is mostly dominated by intact phase. Near failure the behavior is governed by the damaged phase. Then, at any given time, the material is composed of randomly distributed clusters of the material in the intact and damaged phases. Consequently, the observed global response of the material is defined by a combination of the response of the intact part and the response of the damaged part.

Usually, in a material the strains are larger in the damaged part and stresses are higher in the intact part. Due to the stress differential between the damaged and the intact parts a material moment exists, similar to the Coserat and Coserat (1909) continuum definition. Furthermore, due to having different strains in the intact part and in the damaged part there is a relative strain in the material. Modeling the relative strain and the material moment in the solder joint allows us to account for additional energy dissipation mechanisms. The DSC therefore represents an accurate characterization of energy dissipation systems by allowing for the incorporation of microstructural mechanisms in the material.

A treatise of the DSC is given in Desai (1995), Desai et al. (1997) and Basaran et al. (1998a). The DSC assumes that equilibrium of stresses in a material is reached by intact and the damaged phases carrying their share according to the theory of means given by,

$$\sigma_{ij}^{\mathrm{a}} - (1-D)\sigma_{ij}^{\mathrm{i}} + D\sigma_{ij}^{\mathrm{c}}, \tag{1}$$

where σ_{ij}^{a} is the average stress, σ_{ij}^{i} and σ_{ij}^{c} are the stresses carried by the intact and damaged parts, respectively, and D is the isotropic damage. It should be pointed out that converting Eq. (1) to tensorial definition of damage is, mathematically, very straight forward. But due to difficulties measuring tensorial damage in the laboratory commonly scalar damage is used. As the damage increases influence of the intact phase on the overall global response decreases and influence of the damaged part increases. This is very similar to the laboratory observed behavior of Pb/Sn solder alloys Frear et al. (1995). Based on Eq. (1) and the incremental theory of plasticity, Hill (1950), the following incremental stress–strain relation can be obtained (Basaran, 1998),

$$\mathrm{d}\sigma_{ij}^{\mathrm{a}} = C_{ijkl}^{\mathrm{DSC}}\,\mathrm{d}\varepsilon_{kl}^{\mathrm{intact}}, \tag{2}$$

where $\mathrm{d}\sigma_{ij}^{\mathrm{a}}$ is the incremental average stress tensor, $\mathrm{d}\varepsilon_{kl}^{\mathrm{intact}}$ is the incremental strain tensor for the intact part, and the DSC tangential constitutive tensor is given by,

$$C_{ijkl}^{\mathrm{DSC}} = \left[(1-D)C_{ijkl}^{\mathrm{intact}} + (1+\omega)D\,C_{ijkl}^{\mathrm{damaged}} + (\sigma_{ij}^{\mathrm{damaged}} - \sigma_{ij}^{\mathrm{intact}})R_{kl}\right], \tag{3}$$

$$R_{\mathrm{st}} = \frac{\left[D_u A Z \xi_D^{Z-1}\,\exp(-A\xi_D^Z)\right](\partial F/\partial\sigma_{uv})C^{\mathrm{e}}uvst\left((\partial F/\partial\sigma_{ij})(\partial F/\partial\sigma_{ij}) - \frac{1}{3}(\partial F/\partial\sigma_{ij})(\partial F/\partial\sigma_{ij})\right)^{0.5}}{\left[(\partial F/\partial\sigma_{mn})C^{\mathrm{e}}mnpq(\partial F/\partial\sigma_{pq}) - (\partial F/\partial\xi)((\partial F/\partial\sigma_{mn})(\partial F/\partial\sigma_{mn}))^{0.5}\right]}, \tag{4}$$

$C_{ijkl}^{\mathrm{intact}}$ and $C_{ijkl}^{\mathrm{damaged}}$ are the tangential constitutive tensors for the intact and damaged parts, respectively, $\sigma_{ij}^{\mathrm{intact}}$ and $\sigma_{ij}^{\mathrm{damaged}}$ are the stress tensors for the intact and damaged parts, respectively, and ω is the empirical relative strain coefficient.

In the DSC it is assumed that the initial intact material changes its microstructural configuration continuously through a process of self-organization (Bak and Tang, 1989; Aifantis, 1989; Valanis, 1998) and it approaches the damaged state. As the effect of the intact material on the overall response decreases, the effect of the damaged part increases. The transformation from the intact state to the damaged state is defined through a damage evolution function. There is no universally accepted metric to quantify damage in materials or structures. In traditional Kachanov (1986) continuum damage mechanics plastic strain is used as the damage metric. If the plastic strain trajectory is used as the damage metric, a Weibull type damage evolution function can be given by (Basaran et al., 1998a):

$$D + \left(1 - \mathrm{e}^{-A_d\xi_D^Z}\right), \tag{5}$$

A_d and Z are material constants and $\xi_D = \int \sqrt{\mathrm{d}e^{\mathrm{p}}_{ij}\,\mathrm{d}e^{\mathrm{p}}_{ij}}$ is the trajectory of the deviatoric plastic strain. Several researchers have shown that plastic strain trajectory as a damage metric can lead to misleading results (Dasgupta et al., 1992). Yan (1997) and Basaran and Yan (1998), to appear) have shown that the damage in the system can be quantified, more accurately, using the entropy [which is a measure of the disorder] of the system. If the entropy is used as a damage metric the following damage evolution function can be used (Basaran and Yan, to appear):

$$D = 1 - \exp\left(-\frac{\Delta e - \Delta\phi}{N_0 k\theta/\bar{m}_{\mathrm{s}}}\right), \tag{6}$$

where

$$\Delta e - \Delta\phi = \frac{1}{\rho}\left(\int_{\varepsilon_0}^{\varepsilon} \sigma_{ij}\,\mathrm{d}\varepsilon^{\mathrm{p}}_{ij}\right) - \int_{t_0}^{t} \frac{1}{\rho}\vec{q}\cdot\vec{\nabla}\,\mathrm{d}t + \int_{t_0}^{t}\dot{\gamma}\,\mathrm{d}t, \tag{7}$$

where e is the internal energy, ϕ is the Helmholtz free energy, N_0 is the Avagadro's number, k is the Boltzmann's constant, $\bar{m}_{\mathrm{s}}$ is the specific mass, ρ is the material density, σ_{ij} is the stress tensor for the intact part, $\mathrm{d}\varepsilon^{\mathrm{p}}_{ij}$ is the incremental inelastic strain tensor, $\vec{q}$ is the heat flow vector, $\vec{\nabla}$ is the Nabula's vector operator, $\dot{\gamma}$ is the heat production rate of unit mass quantity and $\mathrm{d}t$ is the increment of time.

In this study damage criteria given by Eqs. (5) and (6) have both been implemented and used. It is our experience that damage quantification based on entropy yields better results. Discussion on this subject is presented in Basaran and Yan (to appear).

The first term in Eq. (3) gives the Kachanov (1986) continuum damage mechanics formulation. The second term in the equation accounts for the energy dissipated by the material due to the different strains in the intact part and in the damaged part. The third term in Eq. (3) indicates different stresses in the two parts and includes a material moment effect due to the stress differential.

In any inelastic analysis based on the incremental theory of plasticity, there is a need for a yield criterion to distinguish elastic and inelastic behavior of the material during loading and unloading. The yield surface, F, used in the proposed constitutive model is given by,

$$F = \frac{J_{2\mathrm{D}}}{P_{\mathrm{a}}^2} - \left[\alpha(\theta)\left(\frac{J_1 + R(\theta)}{P_{\mathrm{a}}}\right)^2\right], \tag{8}$$

where J_1 is the first invariant of the total stress tensor, $J_{2\mathrm{D}}$ is the second invariant of the deviatoric stress tensor, P_{a} is the atmospheric pressure, $R(\theta)$ is the material bonding stress, and α is the hardening parameter given by $\alpha = a_1/\xi^{\eta_1}$, where a_1 and η_1 are material constants and $\xi = \int \sqrt{\mathrm{d}\varepsilon^{\mathrm{p}}_{ij}\,\mathrm{d}\varepsilon^{\mathrm{p}}_{ij}}$ is the trajectory of total plastic strain. The yield surface given by Eq. (8) is a modified version of von Mises criterion.

3. Formulation of the thermo-elasto-viscoplasticity

The Pb40/Sn60 solder alloys have a very low melting point (183°C). They experience high homologous temperature during service, as a result they undergo time, temperature and rate dependent deformation process. A thermo-viscoplastic formulation is, therefore, essential for modeling Pb/Sn solder behavior (Basaran, 1996).

Assuming small strain deformations, the strain increment for a thermo-elasto-viscoplastic problem can be separated into three parts,

$$d\varepsilon_{ij} = d\varepsilon_{ij}^{\theta} + d\varepsilon_{ij}^{e} + d\varepsilon_{ij}^{vp}, \tag{9}$$

where $d\varepsilon_{ij}^{\theta}$, $d\varepsilon_{ij}^{e}$ and $d\varepsilon_{ij}^{vp}$ are the incremental thermal, elastic and viscoplastic strain tensors, respectively. Some researchers distinguish the time independent instantaneous plastic deformations from time dependent plastic deformations. Hence, they also add an incremental time-independent plastic strain tensor term to Eq. (9). The drawback of the latter approach is that in the laboratory during testing it is not physically possible to distinguish between the time independent and the time dependent plastic deformations, since in real life everything is time dependent.

In Eq. (9) first two strain components are easily obtained from thermal-elastic deformation relations using coefficient of thermal expansion and Hook's law. Experimental results indicate that the contribution of the elastic strain components to low cycle fatigue life is negligible compared to the contributions of creep strain. The third component in Eq. (9) is the time dependent creep strain which dominates the low cycle fatigue life of solder joints (Solomon, 1986b; Ju et al., 1994). In order to model primary, secondary and tertiary creep stages of Pb/Sn solder alloys several creep rate functions have been proposed in the literature. The viscoplastic strain rate function defined by Perzyna (1966) has been used to model secondary (a.k.a steady-state) creep stage by many researchers (Basaran et al., 1998a, b; Ju et al., 1994, and others):

$$\dot{\varepsilon}_{ij}^{vp} = \Gamma \left\langle \Psi\left(\frac{F}{F_0}\right) \right\rangle \frac{\partial F}{\partial \sigma_{ij}}, \tag{10}$$

where Γ is a material fluidity parameter, F is the yield function given by Eq. (8) and F_0 is a reference stress state, e.g. uniaxial yield stress, and σ_{ij} is the total stress tensor. The function $\Psi(F/F_0)$ is a positive monotonically increasing function determined from experimental data and is given by a power law as follows:

$$\left\langle \Psi\left(\frac{F}{F_0}\right) \right\rangle = \begin{cases} 0 & \text{if } F \leqslant 0, \\ \left(\frac{F}{F_0}\right)^N & \text{if } F > 0, \end{cases} \tag{11}$$

where N is a material constant.

Perzyna's strain rate function given by Eq. (10) does not account for grain size and temperature dependent creep activation energy and power law break down region of creep. It is well known that grain size and temperature make a significant difference in solder alloy behavior and creep behavior of solder is controlled by climb and glide of dislocations. Such a deformation mechanics can be modeled better with a creep rate relation introduced by Sherby (1962) and improved by Garafalo (1965) to include sinh term to account for thermally activated dislocation creep model (Ozmat, 1990). Kashyap and Murty (1981) have shown that including the grain size in strain rate function is essential. In this study the following strain rate function was adopted for multiaxial stress condition:

$$\dot{\varepsilon}_{ij}^{vp} = A(\sinh B\bar{\sigma})^n (d)^m \exp(-Q/R_g T) \frac{\partial F}{\partial \sigma_{ij}}, \tag{12}$$

$$\bar{\sigma} = \sqrt{3J_{2D}}, \tag{13}$$

where J_{2D} is the second invariant of the deviatoric stress tensor, d is the grain size, Q is the apparent creep activation energy (temperature dependent), R, is the gas constant, T is the absolute

temperature, F is the yield surface, σ_{ij} is the stress tensor, A, B, n, and m are material constants. Material constants are obtained from experimental creep data for different grain sizes and strain rates. In this study both Eqs. (10) and (12) were used. It was our finding that Eq. (12) yields much better results for solder alloys.

4. Finite element procedure implementation

The constitutive model was implemented in a finite element procedure. For the displacement based finite element method, the equilibrium equation in incremental form is given by Bathe (1996):

$$\int_V [B]^{\mathrm{T}} \{\mathrm{d}^r \sigma^{\mathrm{a}}_{n+1}\}\, \mathrm{d}V = \{Q_{n+1}\} - \int_V [B]^{\mathrm{T}} \{{}^{r-1}\sigma_n\}\, \mathrm{d}V, \tag{14}$$

where $[B]$ is the strain-displacement transformation matrix, $\{\mathrm{d}\sigma^{\mathrm{a}}\}$ is the vector of average stress increments, V is volume, n is the load step number and r is the iteration number, $\{Q_{n+1}\}$ is the vector of nodal external loads. Implementing the DSC formulation in Eq. (14) yields,

$$\begin{aligned}
&\int_V [B]^{\mathrm{T}} [{}^r L_n^{\mathrm{evp}\theta}][B]\, \mathrm{d}V \{\mathrm{d}^r q_{n+1}\} \\
&\quad = \{Q_{n+1}\} - \int_V [B]^{\mathrm{T}} \{{}^{r-1}\sigma^{\mathrm{a}}_n\}\, \mathrm{d}V - \int_V [B]^{\mathrm{T}} \{{}^{r-1}\sigma^{\mathrm{c}}_n - {}^{r-1}\,\sigma^{\mathrm{i}}_n\}\, \mathrm{d}D_n\, \mathrm{d}V \\
&\qquad + \int_V \Delta t_n [B]^{\mathrm{T}} [{}^{r-1} L_n^{\mathrm{evp}\theta}] \{{}^{r-1}\dot{\varepsilon}_n^{\mathrm{vp}\theta}\}\, \mathrm{d}V + \int_V \Delta t \chi\, \mathrm{d}\theta_n [B]^{\mathrm{T}} [{}^r L_n^{\mathrm{evp}\theta}] [{}^{r-1} G_2]_n \{\bar{I}\}\, \mathrm{d}V \\
&\qquad + \int_V \alpha_T\, \mathrm{d}\theta_n [B]^{\mathrm{T}} [{}^r L_n^{\mathrm{evp}\theta}] \{\bar{I}\}\, \mathrm{d}V,
\end{aligned} \tag{15}$$

where $\{\mathrm{d}^r q_n\}$ is the vector of nodal displacement increments, Δt_n is the time increment for viscoplasticity integration, χ is the time integration coefficient for viscoplasticity, $\mathrm{d}\theta$ is the temperature increment, α_{T} is the coefficient of thermal expansion, $\{I\}$ is a unit vector and $[G_2] = [\partial \dot{\varepsilon}^{\mathrm{vp}\theta}/\partial\theta]_n$ and

$$[{}^r L_n^{\mathrm{evp}\theta}] = \left[(1 - D_n)[{}^i_r C_n^{\mathrm{evp}\theta}] + D_n(1+\omega)[{}^c_r C_n^{\mathrm{evp}\theta}]\right]. \tag{16}$$

In order to introduce the dynamic inertia and damping forces into the finite element equation, we can write the equation of motion for the material nonlinear case as follows:

$$[M]\left\{(\ddot{q}_{n+1} + (\ddot{q}_{\mathrm{g}})_{n+1})\right\} + [C]\{\dot{q}_{n+1}\} + [K]\{(q_n + \mathrm{d}q_{n+1})\} = Q_{n+1}, \tag{17}$$

where q, $\dot{q}$, and $\ddot{q}$ are the nodal displacement, velocity and acceleration vectors, respectively, and $\ddot{q}_g$ is the base acceleration vector, $[M]$ is the mass matrix, $[C]$ is the damping matrix and $[K]$ is the stiffness given by,

$$K = \int_V [B]^{\mathrm{T}} [{}^r L_n^{\mathrm{evp}\theta}][B]\, \mathrm{d}V. \tag{18}$$

Eq. (17) can be rewritten as follows,

$$[M]\{\ddot{q}_{n+1}\} + [C]\{\dot{q}_{n+1}\} + [K]\{\mathrm{d}q_{n+1}\} = \{Q_{n+1}\} - \int_V [B]^{\mathrm{T}}\{\sigma_n^{\mathrm{a}}\}\mathrm{d}V - [M]\{(\ddot{q}_{\mathrm{g}})_{n+1}\} \tag{19}$$

introducing the dynamic terms into Eq. (15) yields,

$$\begin{aligned}
&[M]\{{}^{r}\ddot{q}_{n+1}\} + [{}^{r-1}C_n]\{{}^{r}\dot{q}_{n+1}\} + [{}^{r-1}K_n]\{\mathrm{d}{}^{r}q_n\} \\
&\quad = \{Q_{n+1}\} - \int_V [B]^{\mathrm{T}}\{{}^{r-1}\sigma_n^{\mathrm{a}}\}\,\mathrm{d}V - \int_V [B]^{\mathrm{T}}\{{}^{r-1}\sigma_n^{\mathrm{c}} - {}^{r-1}\sigma_n^{\mathrm{i}}\}\,\mathrm{d}D_n\,\mathrm{d}V \\
&\qquad + \int_V \Delta t_n [B]^{\mathrm{T}}\left[{}^{r-1}L_n^{\mathrm{evp}\theta}\right]\left\{{}^{r-1}\dot{\varepsilon}_n^{\mathrm{vp}\theta}\right\}\mathrm{d}V + \int_V \Delta t\chi\,\mathrm{d}\theta_n [B]^{\mathrm{T}}[{}^{r}L_n^{\mathrm{evp}\theta}][{}^{r-1}G_2]_n\{\bar{I}\}\,\mathrm{d}V \\
&\qquad + \int_V \alpha_T\,\mathrm{d}\theta_n [B]^{\mathrm{T}}[{}^{r}L_n^{\mathrm{evp}\theta}]\{\bar{I}\}\,\mathrm{d}V - [M]\{\ddot{q}\}_{n+1}.
\end{aligned} \tag{20}$$

In the study Rayleigh damping was used (Clough and Penzien, 1993),

$$[C] = \alpha[M] + \beta[K], \tag{21}$$

where α and β are Rayleigh damping coefficients and are determined from two unequal frequencies of vibration that have been obtained by doing an eigenvalue analysis in ANSYS general purpose finite element code.

Using Newmark's (implicit) scheme (with coefficients $\delta = \frac{1}{2}$ and $\alpha = \frac{1}{4}$), for a time domain integration of the equation of motion yields the following equation,

$$\begin{aligned}
&\left[[M]\frac{4}{\Delta t_d^2} + [C_n]\frac{2}{\Delta t_d} + \left[{}^{r-1}K_n\right]\right]\{{}^{r}\mathrm{d}q_{n+1}\} \\
&\quad = \{Q_{n+1}\} - \int_V [B]^{\mathrm{T}}[{}^{r-1}\sigma_n^{\mathrm{a}}]\,\mathrm{d}V - \int_V [B]^{\mathrm{T}}\{{}^{r-1}\sigma_n^{\mathrm{c}} - {}^{r-1}\sigma_n^{\mathrm{i}}\}\,\mathrm{d}D_n\,\mathrm{d}V \\
&\qquad + \int_V \Delta t_n [B]^{\mathrm{T}}[{}^{r-1}L_n^{\mathrm{evp}\theta}]\{{}^{r-1}\dot{\varepsilon}_n^{\mathrm{vp}\theta}\}\,\mathrm{d}V + \int_V \Delta t\chi\,\mathrm{d}\theta_n [B]^{\mathrm{T}}[{}^{r}L_n^{\mathrm{evp}\theta}][{}^{r-1}G_2]_n\{\bar{I}\}\,\mathrm{d}V \\
&\qquad + \int_V \alpha_T\,\mathrm{d}\theta_n [B]^{\mathrm{T}}[{}^{r}L_n^{\mathrm{evp}\theta}]\{\bar{I}\}\,\mathrm{d}V - [M]\left[\frac{4}{\Delta t_d^2}(\{{}^{r-1}q_{n+1}\} - \{q_n\}) - \frac{4}{\Delta t_d}\{\dot{q}_n\} - \{\ddot{q}n\}\right] \\
&\qquad - [C]\left[\frac{2}{\Delta t_d}(\{{}^{r-1}q_{n+1}\} - \{q_n\}) - \{\dot{q}_n\}\right] - [M]\{\ddot{q}_{\mathrm{g}}\}_{n+1}.
\end{aligned} \tag{22}$$

Solution procedures and convergence issues related to Eq. (22) are discussed in great detail in Chandaroy (1998).

5. Parametric study; part I

The finite element procedure presented above is used for dynamic analysis of a Pb40/Sn60 solder joint in a surface mount technology microelectronics package, which is made up of a leadless ceramic chip carrier (LCCC) soldered to a printed wiring board (PWB), see Fig. 1. Material properties of the solder are given in Table 1. The LCCC and the PWB are modeled as linear elastic material, and the solder joint is modeled as elasto-viscoplastic material. The material properties for the chip carrier and PWB are as follows: $E_{\mathrm{ceramic}} = 254.9$ GPa,

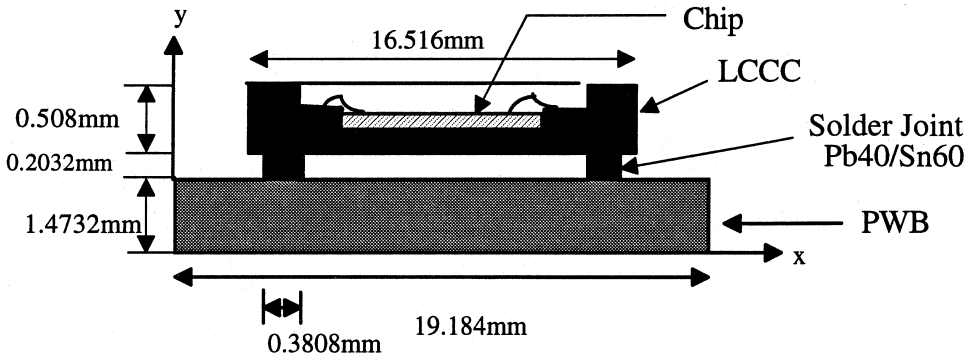

Fig. 1. Schematic section of the surface mount technology package.

Table 1
Pb40/Sn60 material properties

G (MPa)	13.2
v	0.4
a_1	2.9×10^{-6}
η_1	0.620.10.68
ω	0.1
R (GPa)	288
Γ	1.8
N	2.67
A_d	0.1
Z	0.68
A (s^{-1})	2.9524×10^8
B	0.13
m	−3.01
n	1.89
Q (J/mol)	61,417
R_g (J/mol K)	8.314

$v_{\text{ceramic}} = 0.3$, $E_{\text{PWB}} = 12.26$ GPa, $v_{\text{PWB}} = 0.36$. The analysis is conducted for isothermal condition (27°C).

The package is subjected to a simultaneous 2-D base excitation (acceleration) in x and y directions with the time history shown in Fig. 2. In the first part of the parametric study (part I) the LCCC and the PWB were assumed to be massless. In the second part of the study (part II) the LCCC and the PWB were considered with their respective masses. The reason for the massless study was to see behavior of a solder column without interference from modal response of the whole package. Solder joints are used in different types of microelectronic packages with varying geometries. Hence observing solder alloy dynamic response without interference from the package geometry is important and instrumental. It is usually easier to understand behavior of a component as a substructure first and then as a component of the whole structure. This approach is extensively used in soil-structure interaction of structures (Clough and Penzien, 1993). In the second part of the study when the LCCC and the PWB inertias were considered the response of the solder joint was significantly different. This distinction in two phase study was very helpful in understanding that the solder joint behavior can be effected by the geometry and modal frequencies of the package.

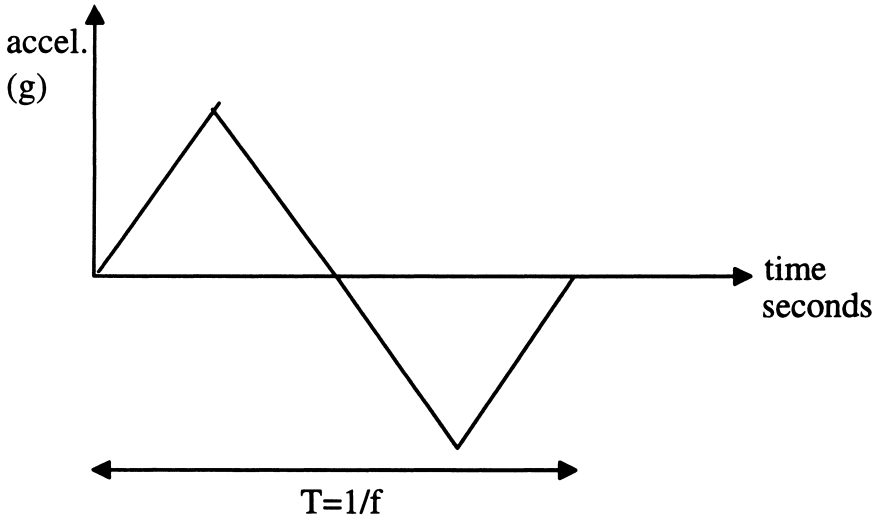

Fig. 2. The time history of the harmonic vibration input.

The parametric study included a wide range of acceleration values, from 20 to 4000 g and frequencies from 10 to 10,000 Hz. For some of the input motions the frequency was high enough to be considered as a shock rather than as a steady state harmonic excitation. The stress–strain and damage response of the solder joint was calculated for each dynamic cycle and by using Miner's rule (Miner, 1945) the accumulative damage was computed. In the study both low cycle and high cycle fatigue were considered. This was essential since under dynamic loading the behavior of the solder alloy can be elastic or inelastic depending on the acceleration and frequency of the vibration. For low cycle fatigue (upto 10^4 cycles, Barker et al., 1990), the damage was calculated using Eqs. (5) and (6). For high cycle fatigue (over 10^4 cycles, Barker et al., 1990), damage was calculated using the following criterion (Barker et al., 1990),

$$D = \sum \frac{n_i}{N_i}, \tag{23}$$

where n_i is the cycles experienced and N_i is the cycles to failure at a specific elastic strain level.

For high cycle fatigue life, test data reported by Steinberg (1988) was used to obtain N_i values. The author presents high cycle fatigue plots for various solders used in electronic equipment. The plots predict the fatigue life ("number of cycles to failure") of the solder (Pb37/Sn63) due to shear stress. The solder joint remains in the elastic region during a high cycle fatigue, hence shear stress can be converted to shear strain using the shear modulus. Steinberg's, test data (Steinberg, 1988) for high cycle fatigue was converted to strain versus cycles to failure by Barker et al. (1990). In this study the data published by Barker et al. (1990) in terms of strain versus number of cycles to failure was used. Barker et al. (1990) used shear modulus $G = 1.91 \times 10^5$ psi from Solomon's data (Solomon, 1986a) to convert the shear stress to shear strain.

In the microelectronics industry the fatigue life of solder joints is always defined in terms of the temperature cycles. Hence, the dynamic load cycles were normalized with respect to temperature cycles (1400 s).

The parametric study results for the first part, where the LCCC and the PWB are assumed massless, indicate that the behavior of the solder joint is elastic for acceleration values, up to 100 g, and frequency range from 10 to 10,000 Hz. Starting from 150 g and going to higher accelerations, inelastic behavior is observed. The behavior of the solder alloy is inelastic starting from

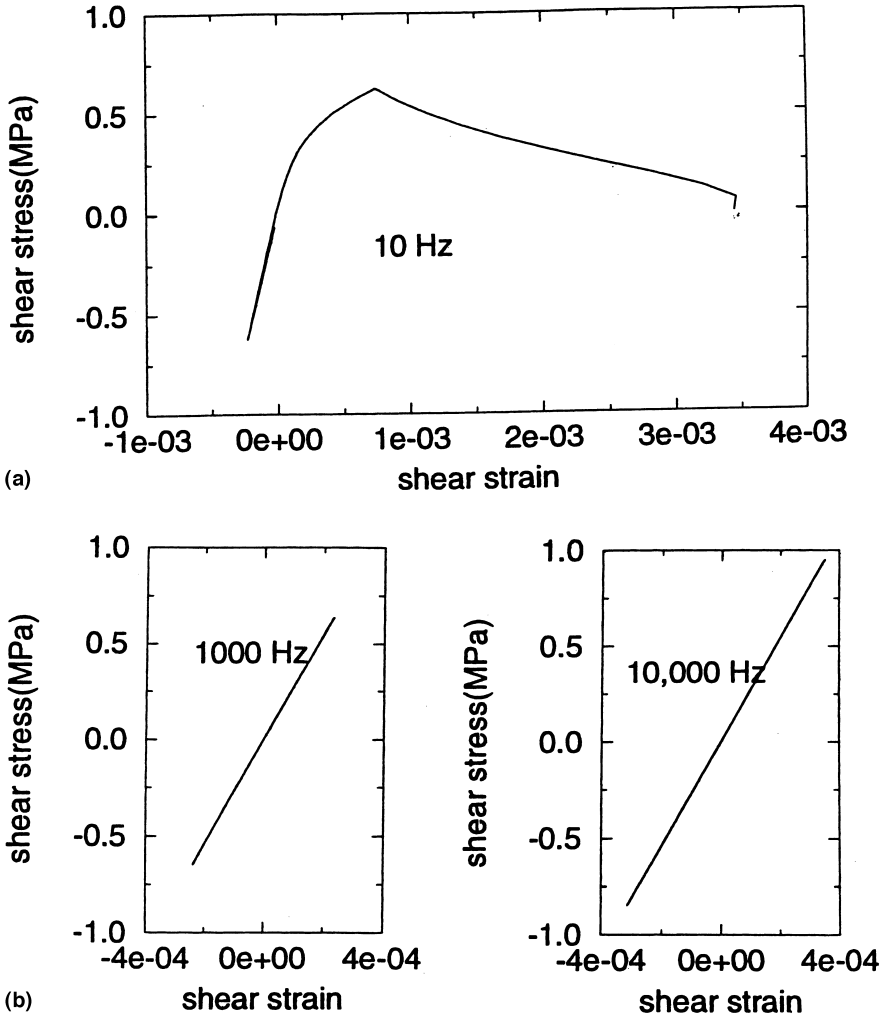

Fig. 3. Shear stress versus shear strain response of solder joint at 150 g.

10 Hz, to about 750 Hz (Fig. 3(a)). The solder joint remains in the elastic range for higher frequencies (Fig. 3(b) and (c)). This observation is consistent with the results reported by Steinberg (1988), "Solder joints that are exposed to low-rate alternating stresses will fail more quickly than solder joints that are exposed to high-rate alternating stresses". This is probably due to the fact that at lower frequencies the period of the load is higher. The time dependent inelastic deformations are directly related to the duration of the load application. For a longer load period, the material has a longer duration to creep. Consequently, for vibrations with small frequencies creep dominates the stress–strain response. From these observations it can be deduced that the frequency of dynamic loading can have a significant effect on the fatigue life of Pb/Sn solder alloys.

It is also observed that when the solder alloy is in the elastic range for 150 g and when frequencies starting from 750 Hz and up occur, the stress level experienced by the material increases as the frequency is increased. The ultimate shear stress level at 10,000 Hz is nearly twice the shear stress at 1000 Hz (Fig. 3(b) and (c)). Yet, when the solder is experiencing viscoplastic strain, the

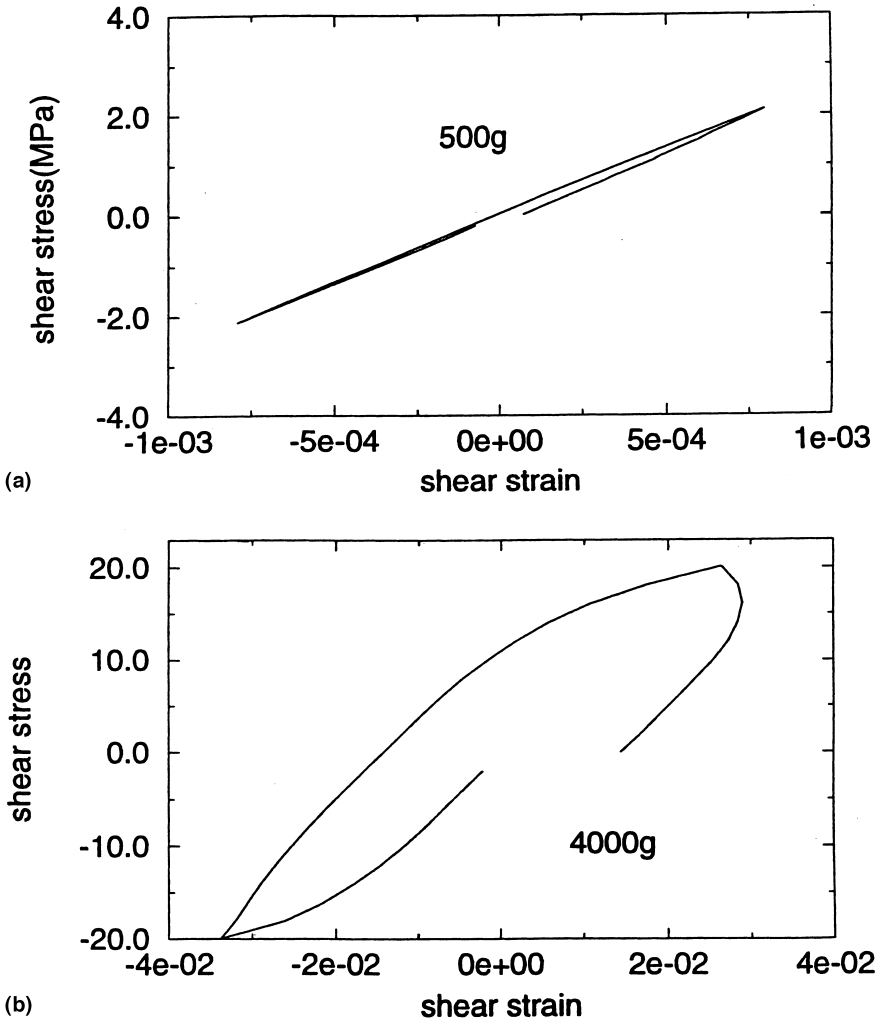

Fig. 4. Shear stress versus shear strain response of solder joint for 500 Hz.

ultimate shear stress level is approximately the same for 10 and 500 Hz. The strain is larger by order of magnitude for 10 Hz than 10,000 Hz.

When the results are analyzed for the same frequency value but for varying acceleration levels, it is observed that at 500 Hz the response is inelastic for acceleration values starting from 150 g, and higher. Fig. 4(a) and (b) show the shear stress versus shear strain response of the Pb40/Sn60 solder joint for one cycle of dynamic loading. The inelastic strain levels and ultimate stress values increase nonlinearly between different acceleration values. For relatively large acceleration values to assume that all vibration induced strains are elastic is not accurate due to the large shear strain values. Shear strain levels for 4000 g at 500 Hz are 40 times larger than shear strain values for 500 g at 500 Hz. Increasing the acceleration eight fold increases shear strain levels by 40 fold.

Fig. 5 shows the damage progress versus the number of thermal cycles for 300 g and 10, 500, and 1500 Hz. The figure indicates that the damage progress is faster for lower frequency vibrations. The number of cycles to failure is relatively low, which indicates that the solder joint is

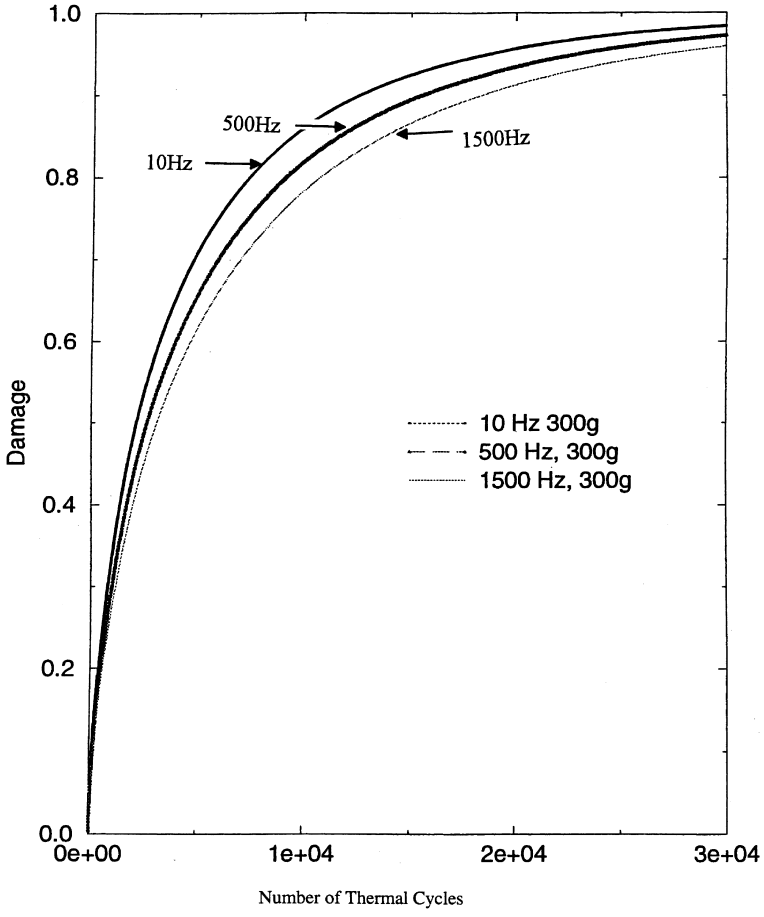

Fig. 5. Damage versus number of thermal cycles in the solder joint for 300 g.

experiencing low cycle fatigue. The fatigue life in this case would be significantly reduced if the ambient temperature were increased (without including the thermal cycling fatigue effects) during this dynamic loading. This curve is a good representation of a significant effect of the damage caused in the solder joint due to dynamic loads. The results suggest that vibrational fatigue damage cannot be ignored or classified as high cycle fatigue only.

The results presented in Fig. 6 indicate that for the same frequency (such as 500 Hz) the larger acceleration causes faster damage accumulation in the material. From the figure it can be deduced that 50% damage accumulation occurs in 10,000 cycles for 300 g loading. On the other hand when the acceleration level is reduced by one-third, the 50% damage accumulation takes five times more thermal cycles to accumulate. This result indicates that the fatigue behavior of P40/Sn60 is highly nonlinear and the damage accumulation and the acceleration level are not linearly dependent.

Fig. 7 depicts the accumulated energy density versus the thermal cycles. Energy density is defined as the area inside the stress–strain hysteresis curve at each cycle. A comparison is presented for the same acceleration value and different loading frequencies. Energy dissipation in a nonconservative system is a mechanism by which the external energy is converted into internal energy as plastic work and heat. Plastic work leads to microstructural reorganization and

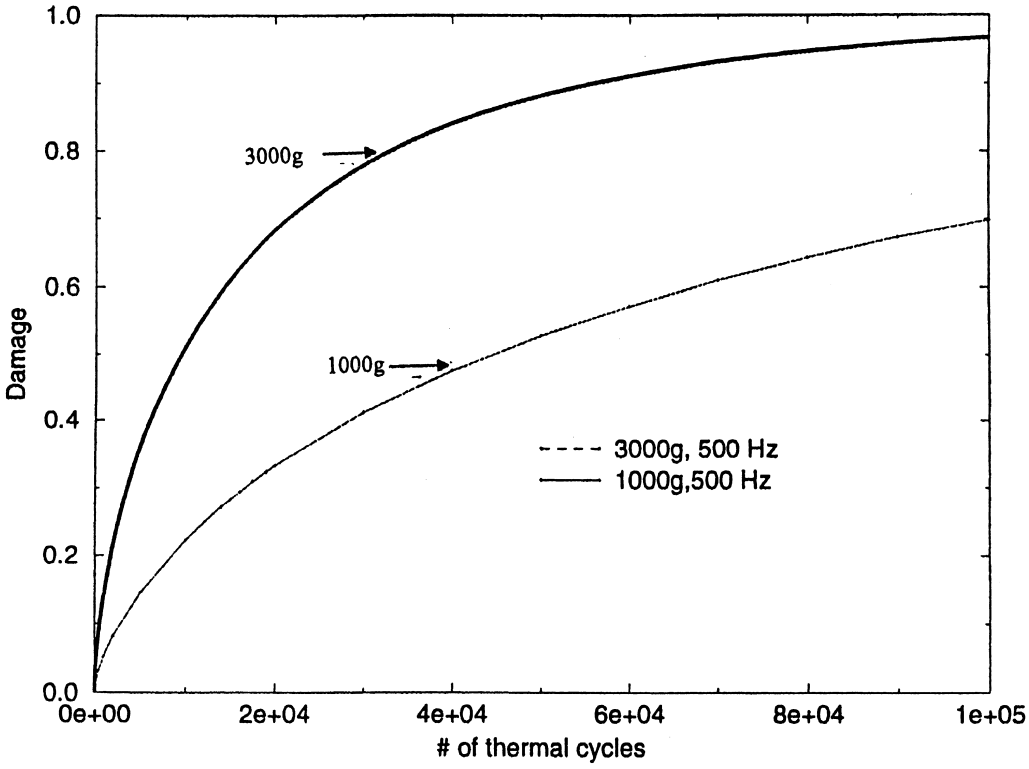

Fig. 6. Damage versus number of thermal cycles for 500 Hz.

microcraking (damage) of the material. Therefore, damage and accumulated energy density are proportional. It is observed that damage accumulation is faster in the lower frequencies. When the behavior of energy density is studied for the same frequency versus different acceleration values, the results indicate that the drop in energy density is much faster for the higher acceleration value. As a result larger acceleration values lead to a shorter fatigue life.

Fig. 8(a) shows the damage experienced in a cycle versus the frequency and the plot is given for different acceleration values. For the acceleration and frequency values given in this figure, the behavior of the solder joint is linear elastic. Hence, the lower frequency loads cause smaller damage per cycle. This is due to the fact that when the acceleration is low enough to cause the solder to remain in the elastic region, the longer periods cannot induce creep damage. When the solder is in the elastic zone, the large frequency values correspond to very small load periods, such as 10,000 Hz for a 0.0001 s period. These loads with very small periods could be considered as shocks. The system experiences larger damage at each cycle as the shock duration is shorter, since the shock becomes more intense. But when the material goes into the viscoplastic range, the creep fatigue dominates the damage value rather than just the shock intensity. This last statement is proven by Fig. 8(b), where the damage per cycle is depicted for different acceleration values. For the acceleration values shown, the solder is experiencing viscoplastic deformations. As a result, for smaller frequencies, the damage experienced in each cycle is bigger.

Fig. 9(a) and (b) show the damage per cycle versus acceleration. The first figure is for the elastic behavior of the solder material. The second figure is for the viscoplastic behavior of the material. When the behavior is elastic smaller frequencies lead to lower damage. Yet, for inelastic behavior, smaller frequencies cause larger damage in each cycle and vice versa.

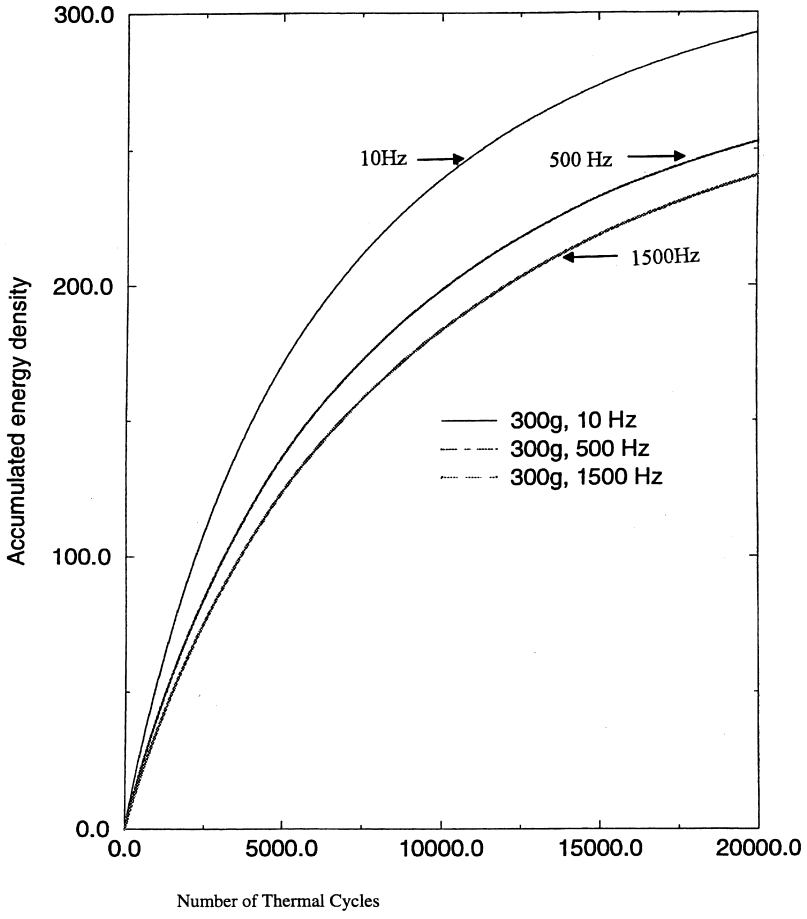

Fig. 7. Accumulated energy density versus number of thermal cycles for 300 g.

6. Parametric study; part II

In this part of the study LCCC and PWB dynamic inertias were taken into account. The grain size effects on solder creep behavior was also considered. The first step of this part of the study was the determination of the natural frequencies and mode shapes of the package. Table 2 shows the natural frequencies of the package assembly for the first ten modes.

Fig. 10(a)–(g) depict the average shear stress versus the average shear strain in the solder joint for 20 g acceleration in the x and the y directions for frequencies from 10 to 1000 Hz. The results indicate that solder joints with larger grain size are more resistant to creep and consequently experience less damage in each cycle. The area inside a stress–strain curve is the energy dissipated in the system. The dissipated energy is proportional to damage experienced. Solder joints with larger grain size have less energy dissipated in each cycle. This observation is consistent with the findings reported by material scientists Morris et al. (1994). It should be pointed out that during service the eutectic solder coarsens (increases in grain size) and its microstructure becomes thermodynamically stable.

For the same grain size smaller frequencies induce bigger damage except in the vicinity of the first mode of the package. Near the resonant frequency the amount of energy dissipated in the solder becomes maximum. As the frequency of the loading gets larger compared to the natural

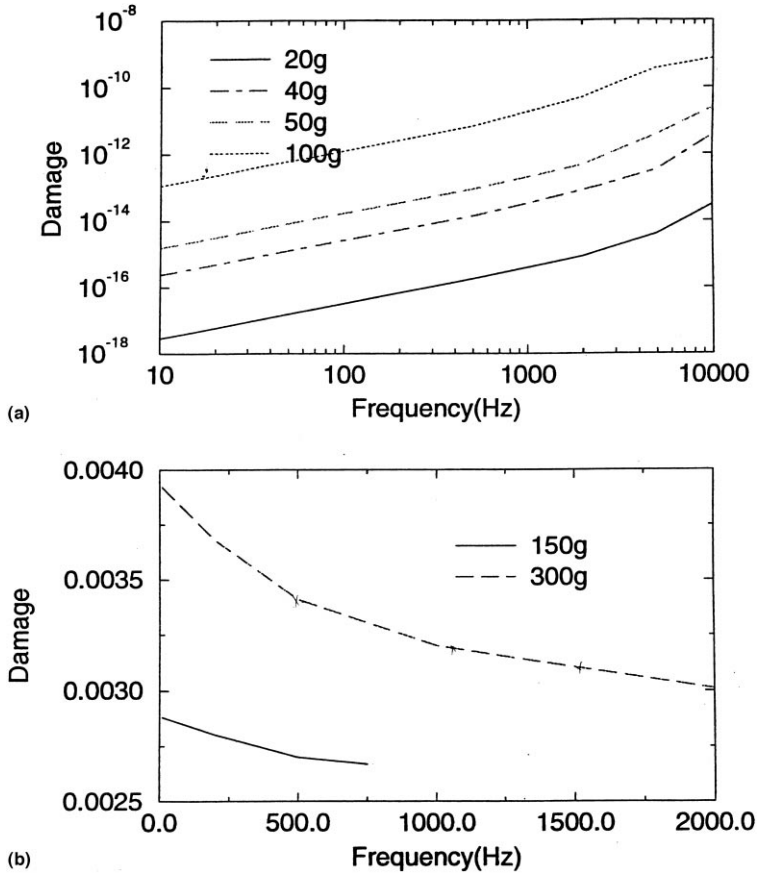

Fig. 8. Damage versus frequency behavior of the solder joint.

frequency of the package the solder experiences less plastic deformations and at 1000 Hz the response is elastic. At frequencies over 1000 Hz the behavior is completely elastic. It should be pointed out that the natural frequency of the package is not affected by the grain size of the solder joint. The solder grain size is a function of cooling rate, temperature history, aging, past deformations and manufacturing process. Therefore it is important to understand that grain size can have a significant impact on the dynamic response of solder joints.

Fig. 11 shows the shear stress versus shear strain response to 30 g acceleration vibrations in the x and the y directions with frequencies ranging from 10 to 1000 Hz for two separate grain sizes 2.5 and 5 μm. The results indicate that compared to 20 g vibrations, the shear strain range experienced is larger by order of a magnitude. This indicates that the relation between acceleration and strain range is highly nonlinear. A 30 g and 1000 Hz vibration the response is inelastic compared to 20 g and 1000 Hz where the response is elastic. This difference is, probably, due to the larger inertia load at 30 g. The over all trend of the joint is very similar to 20 g acceleration results.

Fig. 12 shows the damage versus the frequency response. For the same acceleration values smaller frequencies cause more creep damage but as the frequency of the vibrations get near the fundamental frequency of the package trend changes. Again it is easily observed that damage experienced by the solder joint peaks near the resonant frequency of the package. Comparing

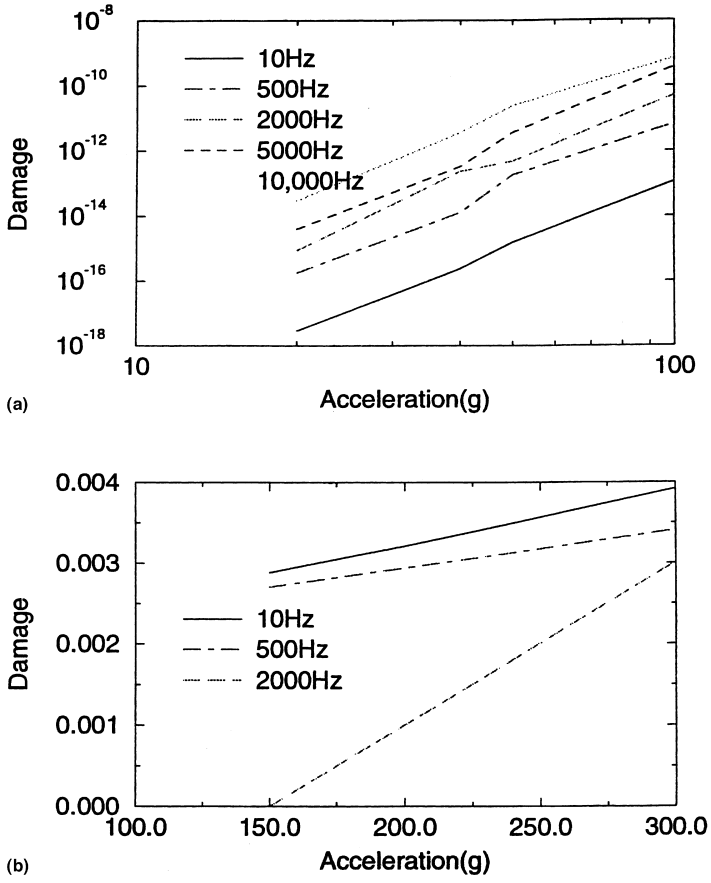

Fig. 9. Damage versus acceleration behavior of the solder joint.

response of solders with different grain sizes we can see that solder alloys with larger grain diameters experience less damage for the same loading.

Fig. 13(a) and (b) depict damage versus number of dynamic cycles for 30 g loading in x–y plane for a solder joint with the average grain size of 2.5 and 5 μm, respectively. Again we observe that damage accumulation is faster for 10 Hz than 100 Hz. But when the frequency gets near the natural frequency transfer function of the system amplifies the response, hence damage experienced by the solder gets larger. Well past the resonant frequency, the damage experienced again becomes lower than 10 Hz. Essentially, when the modal shapes and frequencies of the system is not considered the smaller frequencies induce higher damage, as it was inferred in the part I of this parametric study. Comparing response for 2.5 and 5 μm we notice that the same value of damage is reached in less number of cycles for smaller solder grain sizes.

Table 2
Modal frequencies for the first ten modes

Mode 1	Mode 2	Mode 3	Mode 4	Mode 5	Mode 6	Mode 7	Mode 8	Mode 9	Mode 10
414.8 Hz	785.76 Hz	1257.5 Hz	2800.1 Hz	2838.4 Hz	3680.7 Hz	4909.3 Hz	5194.8 Hz	5290.3 Hz	6399.2 Hz

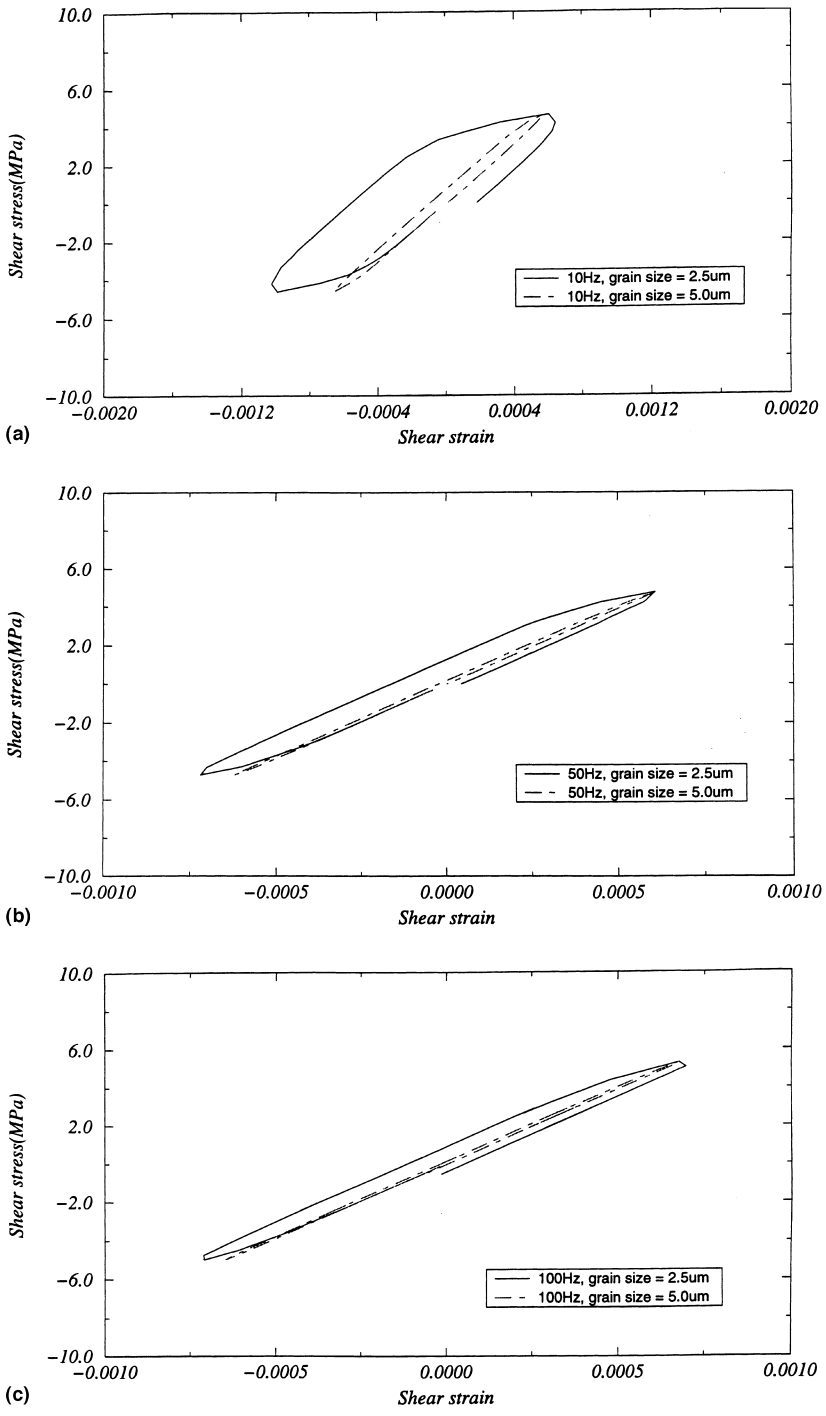

Fig. 10. (a) Stress versus strain response to 20 g acceleration – 10 Hz vibration. (b) Stress versus strain response to 20 g acceleration – 50 Hz vibration. (c) Stress versus strain response to 20 g acceleration – 100 Hz vibration. (d) Stress versus strain response to 20 g acceleration – 500 Hz vibration. (e) Stress versus strain response to 20 g acceleration – 400 Hz vibration. (f) Stress versus strain response to 20 g acceleration – 600 Hz vibration. (g) Stress versus strain response to 20 g acceleration – 1000 Hz vibration.

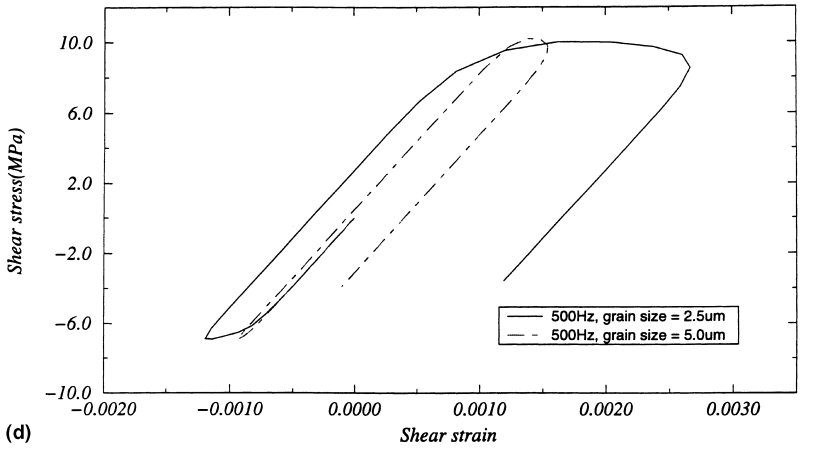

(d)

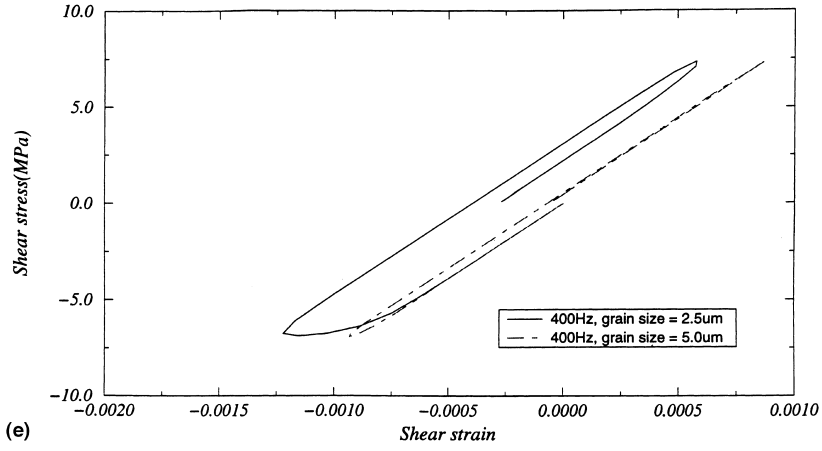

(e)

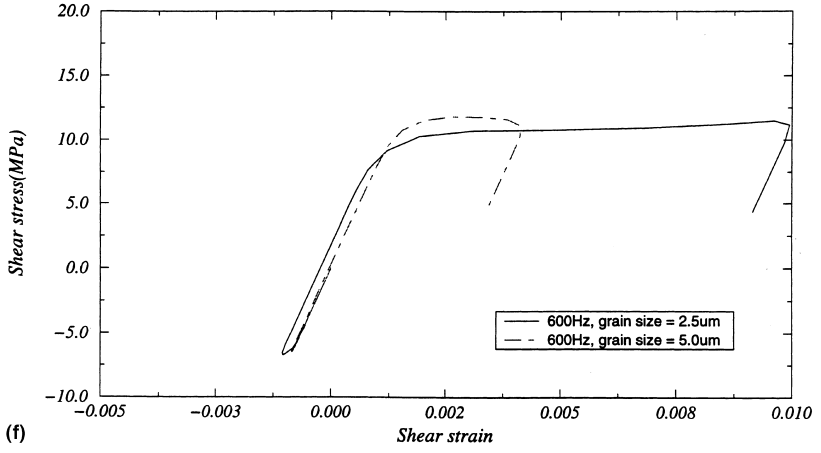

(f)

Fig. 10. (continued).

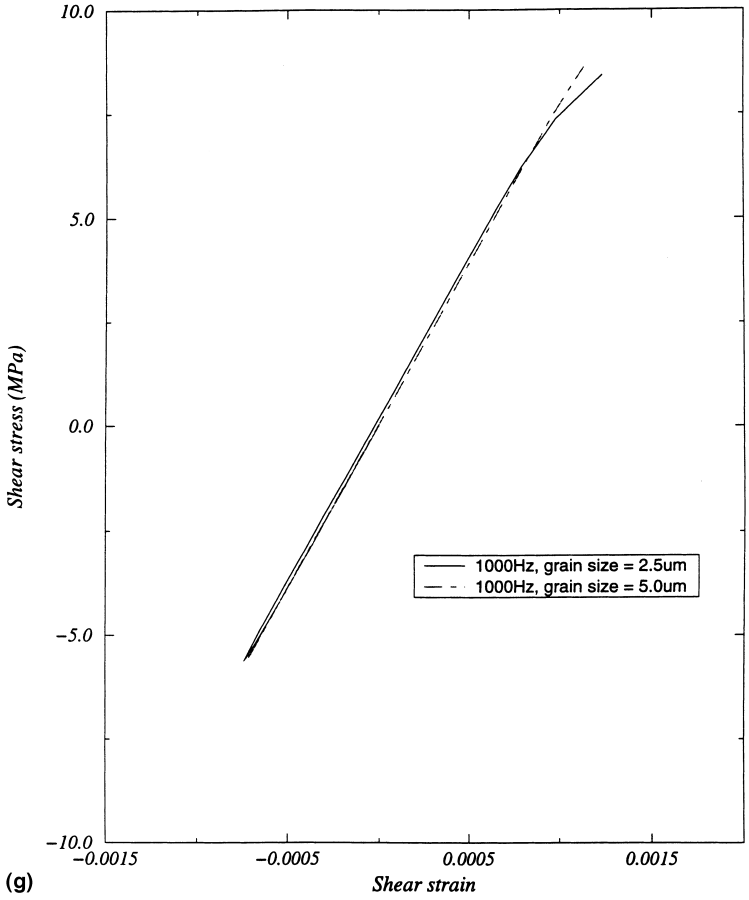

Fig. 10. (continued).

Finally, Fig. 14(a) and (b) present damage versus acceleration for two different grain sizes. It is observed that higher acceleration values induce larger damage in each cycle, but the relation between damage and acceleration is highly nonlinear.

In the literature different definitions of failure have been used for various engineering applications. Discussion of the percentage of damage that constitutes failure is outside the scope of this study.

Having not included the thermal loading in this paper was a deliberate decision. Only having dynamic loading makes an interpretation much easier. It has been reported that having in phase or out of phase thermal loading concurrently with dynamic loading makes a significant difference in the overall response of the Pb40/Sn60 solder.

7. Conclusions

A unified damage mechanics based viscoplastic constitutive model has been implemented in a finite element procedure for time domain dynamic analysis. Incorporating the damage formulation into the constitutive model eliminates the need to perform a stress analysis and a fatigue life analysis separately.

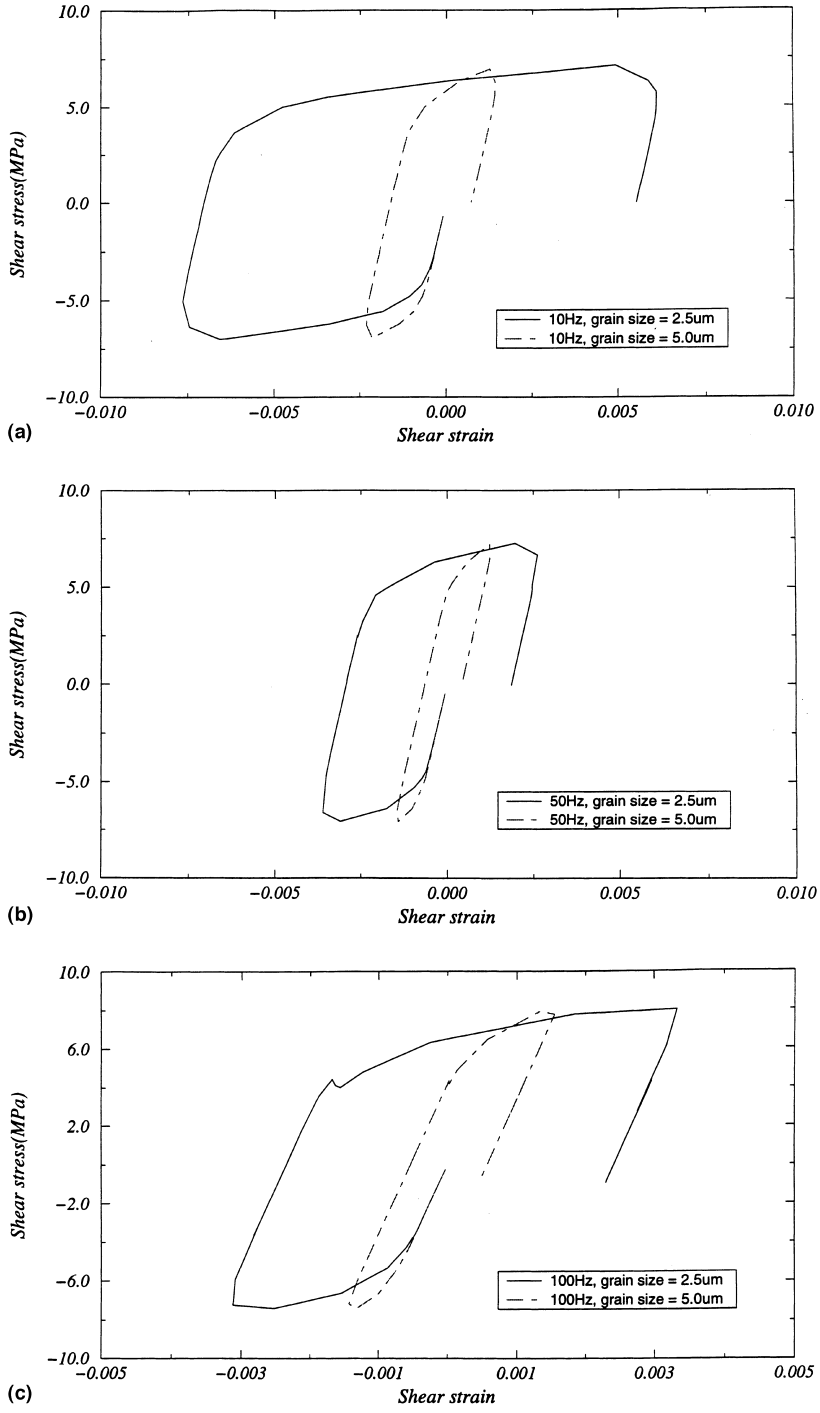

Fig. 11. (a) Stress versus strain response to 30 g acceleration – 10 Hz vibration. (b) Stress versus strain response to 30 g acceleration – 50 Hz vibration. (c) Stress versus strain response to 30 g acceleration – 100 Hz vibration. (d) Stress versus strain response to 30 g acceleration – 400 Hz vibration. (e) Stress versus strain response to 30 g acceleration – 500 Hz vibration. (f) Stress versus strain response to 30 g acceleration – 600 Hz vibration. (g) Stress versus strain response to 30 g acceleration – 1000 Hz vibration.

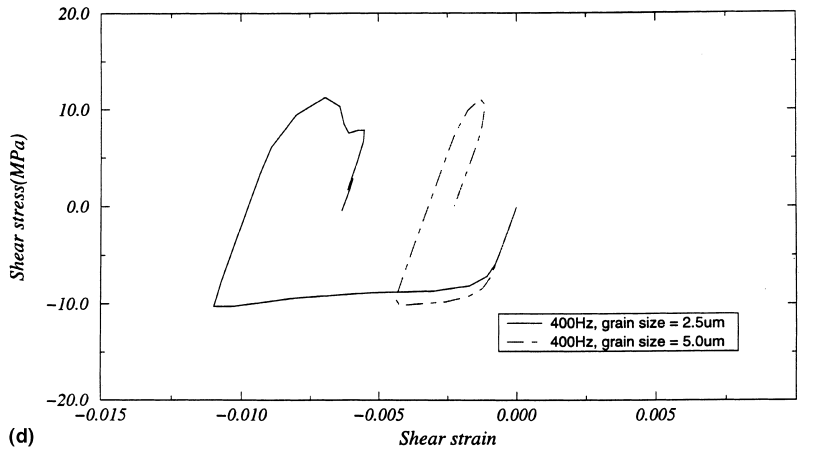

(d)

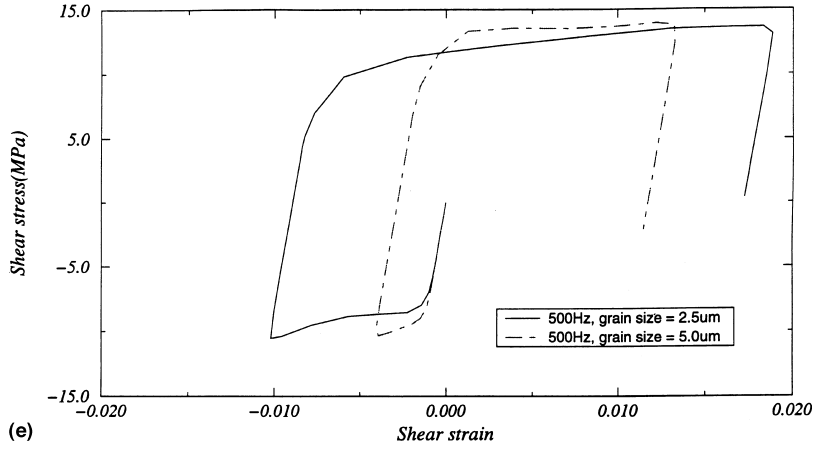

(e)

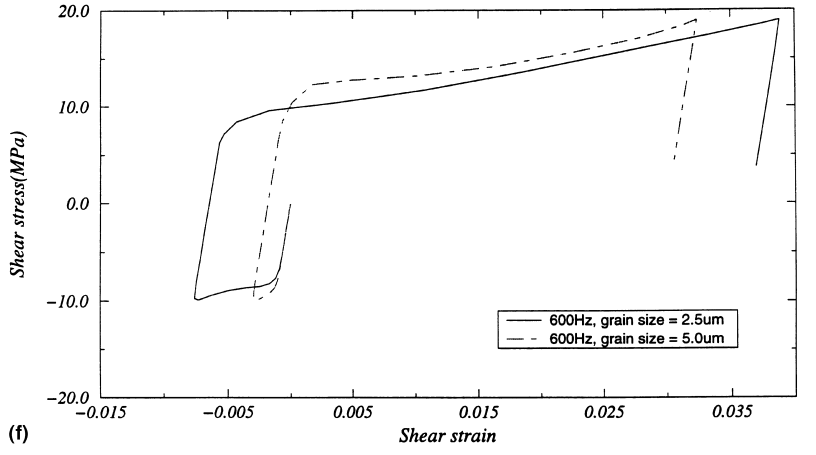

(f)

Fig. 11. (continued).

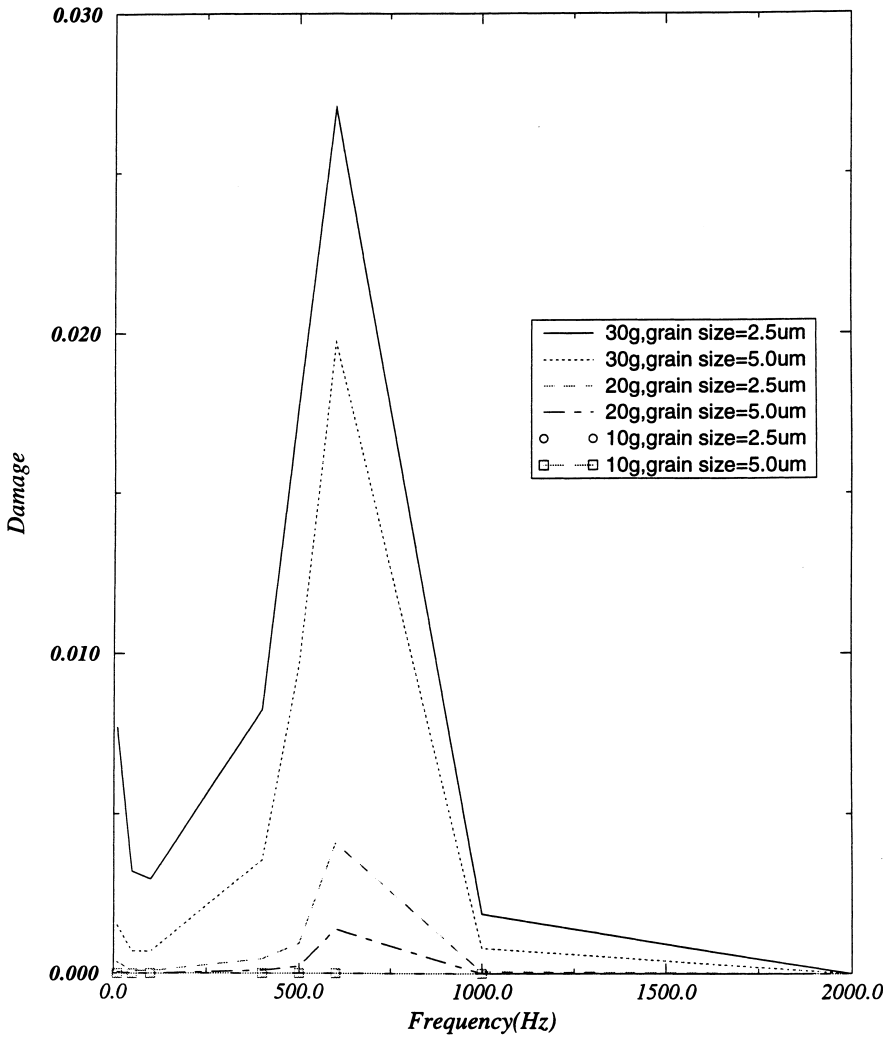

Fig. 12. Damage versus frequency response.

Low- and high-cycle fatigue behavior of a solder joint between a leadless ceramic chip carrier and a printed wiring board has been studied. It has been observed that damage experienced due to vibrations can be significant. Contrary to popular belief, the solder alloy does not remain in the elastic range regardless of the frequency of loading and the acceleration level. When the material is in the elastic range, the higher frequency leads to higher damage in each cycle. But when the solder behavior is inelastic, lower frequency vibrations cause higher damage in each cycle than in higher frequency loads.

When the solder joint experiences inelastic deformations during the vibration, ignoring the damage contributions can lead to significant errors in the determination of the low cycle fatigue life. Vibrations can lead to quick accumulation of fatigue damage. This is due to a high repetition of the vibration cycles in each thermal cycle. The practice of assuming that all vibration induced strains are elastic and ignoring them can lead to serious errors in fatigue life determinations. Most fatigue life analysis procedures employed in the industry are based on the strain range and Coffin–Manson curves. This study has shown that Coffin–Manson type fatigue analysis is invalid when

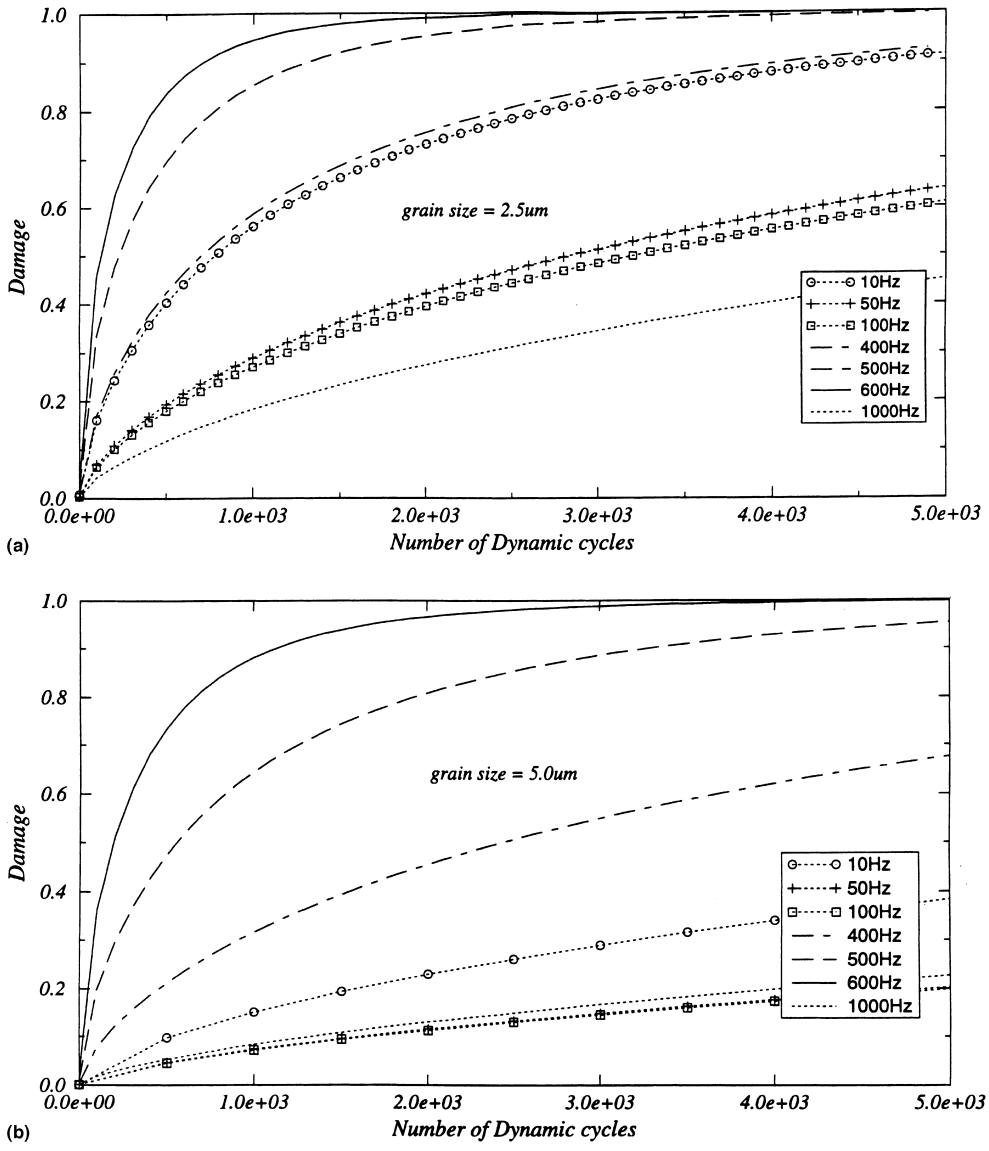

Fig. 13. (a) Damage versus number of dynamic cycles for grain size 2.5 μm. (b) Damage versus number of dynamic cycles for grain size 5 μm.

strains due to vibrations are present. Natural frequency of the microelectronics package significantly affects the response of the solder joint fatigue life.

It should be emphasized that the large number of cycles required for failure in the elastic range could be misleading. When the dynamic load is concurrent with the thermal cycling, the number of cycles to failure is reduced significantly. When the temperature is increased, the viscous effects become stronger and the number of cycles to failure is reduced significantly.

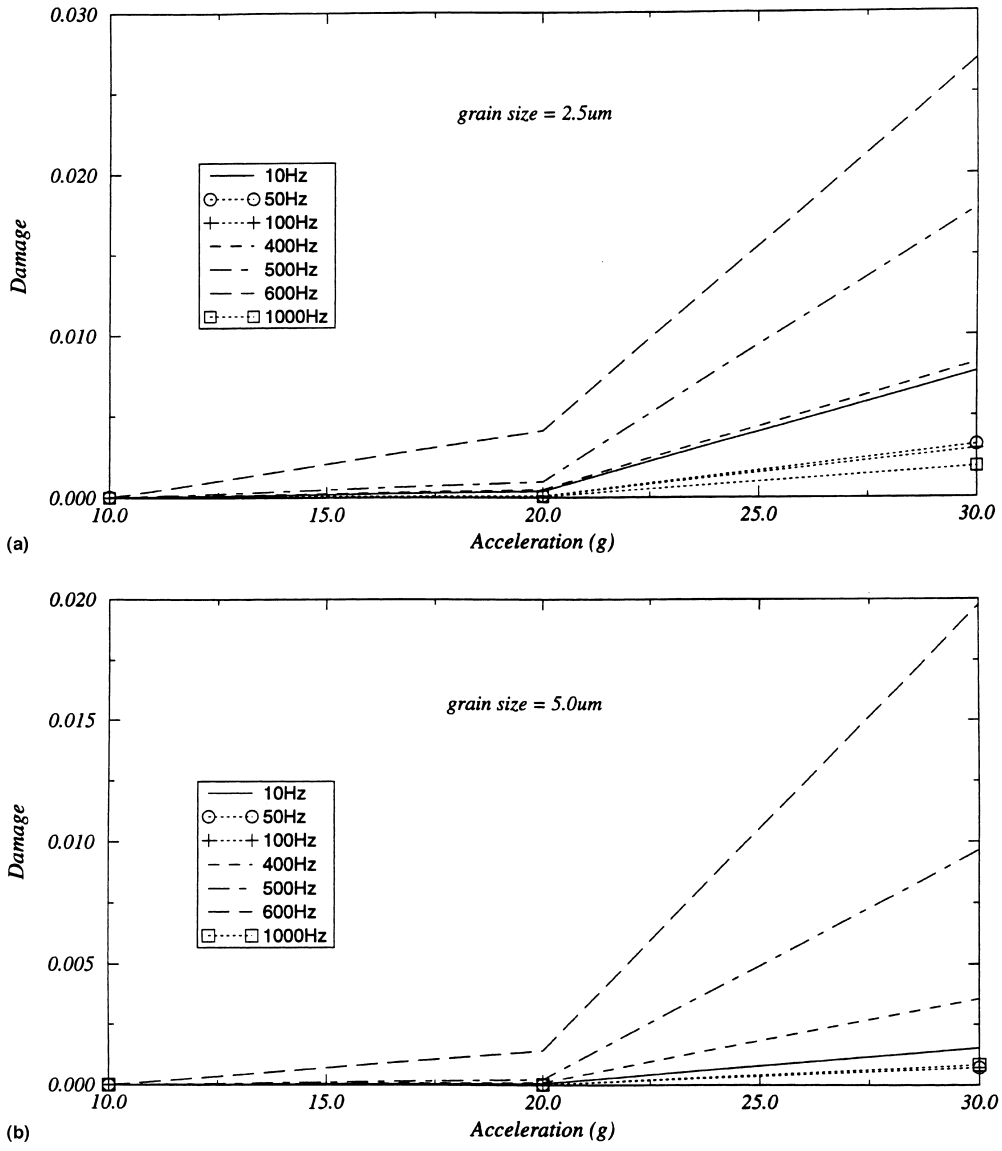

Fig. 14. (a) Damage versus acceleration response for grain size 2.5 μm. (b) Damage versus acceleration response for grain size 5.0 μm.

Acknowledgements

This study was supported by the US Department of Defense Office of Naval Research Young Investigator Award to the first author. Authors are grateful to Dr. Roshdy Barsoum, Director of Solid Mechanics program at ONR for his constructive criticism.

References

ABAQUS, 1996. ABAQUS version 5.6 Hibbit. Karlsson and Sorensen, Inc.
ADINA, 1996. ADINA Users Manual. ADINA Corp., Watertown, MA.

Aifantis, E.C., 1989. Plasticity and self-organization. In: Jinghang, F., Murakami, S. (Eds.), Advances in Constitutive Laws for Engineering Materials. Intern. Academic Publishers, Oxford.
ANSYS, 1992. ANSYS Users Manual Rev. 5. Swanson Analysis Systems, Inc., Houston, PA.
Bak, P., Tang, C., 1989. Earthquake as a self-organized critical phenomenon. J. Geophys. Res. 94 (B11), 15635–15637.
Barker, D.B., Sidharth, 1995. Vibration induced fatigue life estimation of corner leads of peripheral leaded components. In: Proceedings of ASME Congress, San Francisco, CA.
Barker, D., Vodzak, J., Dasgupta, A., Pecht, M., 1990. Combined vibrational and thermal solder joint fatigue – A generalized strain versus life approach. Trans. ASME, J. Electronic Packag. 112, 129–134.
Basaran, C., 1996. A comparison of viscoplastic and plastic constitutive models for solder alloys. In: Suhir, E. (Ed.), Structural Analysis in Microelectronics and Fiber Optics. ASME-EEP-16, 1996, pp. 149–154.
Basaran, C., 1998. Unified disturbed state concept. In: Modeling to Applications in Geomechanics. Wiley, New York.
Basaran, C., Yan, C., 1998. A damage criterion based on entropy. In: Proceedings of the ASCE 12th Engineering Mechanics Conference, La Jolla, CA, 17–20 May.
Basaran, C., Yan, C. A thermodynamic framework for damage mechanics of solder alloys. J. Electronic Packag., Trans. ASME, to appear.
Basaran, C., Desai, C.S., Kundu, T., 1998a. Thermomechanical finite element analysis of problems in electronic packaging using the disturbed state concept. Part I: Theory and formulation. J. Electronic Packag. 120 (1), 41–47.
Basaran, C., Desai, C.S., Kundu, T., 1998b. Thermomechanical finite element analysis of problems in electronic packaging using the disturbed state concept. Part II: Verification and application. J. Electronic Packag. 120 (1), 48–54.
Bathe, K.J., 1996. Finite Element Procedures. Prentice-Hall, Engelwood Cliffs, NJ.
Blanks, H.S., 1976. Accelerated vibration fatigue testing of leadless and solder joint. In: Microelectronics and Reliability, vol. 15. Pergamon Press, Oxford, pp. 213–219.
Bonda, N.R., Noyan, I.C., 1996. Effect of the specimen size in predicting the mechanical properties of PbSn solder alloys. Trans. Comp. Pack. and Manuf. Tech. A 19 (2).
Chandaroy, R., 1998. Damage Mechanics of Solder Joints Under Combined Dynamic and Thermal Loading. Ph.D. Dissertation, Dept. of Civil Engineering, SUNY at Buffalo.
Clough, R.W., Penzien, J., 1993. Dynamics of Structures. McGraw-Hill, New York.
Coserat, E., Coserat, F., 1909. Theorie des Corps Deformables. Herman, Paris.
Darbha, K., Ling, S., Upadhyayula, K., Dasgupta, A., 1996. Stress Analysis of Surface-Mount Interconnects Due to Vibrational Loading, ASME, WAM, Atlanta, GA.
Dasgupta, A., Oyan, C., Barker, D., Pecht, M., 1992. Solder creep-fatigue analysis by an energy-partitioning approach. Trans. ASME, J. Electronic Packag. 114.
Desai, C.S., 1995. Constitutive modeling using the disturbed state as microstructure, self-adjustment concept. In: Muhlhaus, H.B. (Ed.), Continuum Models for Materials with Microstructure, Chap. 8. Wiley, New York.
Desai, C.S., Chia, J., Kundu, T., Prince, J., 1997. Thermomechanical response of materials and interfaces in electronic packaging: Part I: Unified constitutive model and calibration. J. Electronic Packag. 119 (4), 294–300.
Frear, D., Morgan, H., Burchett, S., Lau, J., 1994. The Mechanics of Solder Alloy Interconnects. Chapman & Hall, New York.
Frear, D.R., Burchet, S.N., Rashid, M.M., 1995. A microstructurally based model of solder joints under conditions of thermomechanical fatigue. In: Advances in Electronic Packaging. ASME, EEP-Vol. 10, pp. 347–360.
Garafalo, F., 1965. Fundamentals of Creep and Creep-Rupture in Metals. McMillan, New York.
Hill, R., 1950. The Mathematical Theory of Plasticity. Oxford University Press, Oxford.
Ju, S.H., Kuskowski, S., Sandor, B.I., Plesha, M.E., 1994. Creep-fatigue damage analysis of solder joints. In: Schroeder, S.A., Mitchell, M.R. (Eds.), Fatigue of Electronic Materials, ASTM STP, 1153. American Society for Testing and Materials, Philadelhia, PA, pp. 1–21.
Kachanov, L.M., 1986. Introduction of Continuum Damage Mechanics. Nijhoff (Martinus), Dordrecht.
Kashyap, P., Murty, G.S., 1981. Experimental constitutive relations for the high temperature deformation of a Pb–Sn eutectic alloy. J. Mater. Sci. Eng. 50, 205–213.
Knecht, S., Fox, L.R., 1990. Constitutive relation and creep-fatigue life model for eutectic tin–lead solder. IEEE Trans. Comp. Hybr. Manuf. Tech. 13 (2), 424–433.
Lau, J., Schneider, E., Baker, T., 1995. Shock and vibration of solder bumped flip chip on organic coated copper boards. In: Proceedings of the ASME International Mechanical Engineering Congress and Exposition, San Francisco, CA.
Markstein, H.W., 1987. Designing electronics for high vibration and shock. J. Electronic Packag. Production, Special Report, April, 40–43.

Miner, M.A., 1945. Cumulative damage in fatigue. J. Appl. Mech. 12 (September).
MIL-HDBK-304, 1964. Military Standardization Handbook Package, Cushioning Design. Department of Defense, Washington, DC.
Morris, J.W. Jr., Reynolds, H.L., 1992. The influence of microstructure on the mechanics of eutectic solders. EEP-Vol. 19-2, Advances in Electronic Packaging.
Morris, J.W., Goldstein, F.J.L., Mei, Z., 1994. Microstructural influences on mechanical properties of solder. In: Frear, D. et al. (Eds.), The Mechanics of Solder Alloy Interconnects, Chap. 2. Chapman & Hall, New York.
Ozmat, B., 1990. A nonlinear thermal stress analysis of surface mount solder joints. In: Proceedings of 40th Electronic Components and Technology Conference, Las Vegas, Nevada, 20–23 May.
Perzyna, P., 1966. Fundamental problems in visco-plasticity. In: Recent Advances in Applied Mechanics. Academic Press, New York.
Pitarresi, J.M., Akanda, A., 1993. Random vibration response of a surface mount lead/solder joint. In: Advances in Electronic Packaging. ASME-EEP-Vol. 4-1.
Sherby, O.D., 1962. Acta Metallurgica 10, 135–147.
Solomon, H.D., 1986a. Fatigue of 60/40 solder. IEEE Trans. Components Hybrids Manufacturing Technol. CHMT–9 (4), 423–432.
Solomon, H.D., 1986b. Creep, strain-rate-sensitivity and low cycle fatigue of 60/40 solder. Brazing and Soldering 11, 68–75.
Steinberg, D.S., 1988. Vibration Analysis for Electronic Equipment. Wiley, New York.
Stone, D.S., Rashid, M.M., 1994. Constitutive Models. In: Frear, D. et al. (Eds.), The Mechanics of Solder Alloy Interconnects, Chap. 4. Chapman & Hall, New York.
Suhir, E., Lee, Y.C., 1988. Thermal, mechanical, and environmental durability design methodologies. In: Electronic Materials Handbook, vol. 1. ASM International.
Valanis, K.C., 1998. A gradient thermodynamic theory of self-organization. Acta Mechanica 127, 1–23.
Yan, C.Y., 1997. A Damage Mechanics Based General Purpose Interface/Contact Element. Ph.D. Dissertation, Dept. of Civil, Structural and Environmental Engineering, SUNY at Buffalo.